Spin-orbit torques in perpendicularly magnetized $Ir_{22}Mn_{78}/Co_{20}Fe_{60}B_{20}/MgO$ multilayer

Di Wu,[1,2] Guoqiang Yu,[1,a)] Ching-Tzu Chen,[3] Seyed Armin Razavi,[1] Qiming Shao,[1] Xiang Li,[1] Bingcheng Zhao,[2] Kin L. Wong,[1] Congli He,[1] Zongzhi Zhang,[2] Pedram Khalili Amiri,[1,4] and Kang L. Wang[1]

[1]*Department of Electrical Engineering, University of California, Los Angeles, California 90095, USA*
[2]*Key Laboratory of Micro and Nano Photonic Structures (Ministry of Education), Department of Optical Science and Engineering, Fudan University, Shanghai 200433, China*
[3]*IBM Thomas J Watson Research Center, Yorktown Heights, New York 10598, USA*
[4]*Inston Inc., Los Angeles, California 90095, USA*

(Received 5 August 2016; accepted 9 November 2016; published online 28 November 2016)

The current-induced spin-orbit torques (SOTs) in the perpendicularly magnetized $Ir_{22}Mn_{78}/Co_{20}Fe_{60}B_{20}/MgO$ structures are investigated. The damping- and field-like torques are characterized using a harmonic technique. The spin Hall angle of $Ir_{22}Mn_{78}$ is determined to be $\theta_{SHE} = +0.057 \pm 0.002$. The SOT-driven magnetization switching is also demonstrated with the assistance of an external in-plane field. Furthermore, the magneto-optical Kerr effect imaging experiments show that the magnetization switching is realized through domain nucleation and domain wall motion. These results may promise potential practical applications in high-performance SOT devices based on the antiferromagnetic materials. *Published by AIP Publishing.* [http://dx.doi.org/10.1063/1.4968785]

Spin-orbit torque (SOT) has attracted considerable attention as a potential write method for switching perpendicular magnets in magnetic memories, which allows for a lower write energy compared with the conventional spin-transfer torques.[1–4] A commonly studied SOT device is based on a perpendicularly magnetized stack consisting of heavy metal (HM)/ferromagnet (FM)/insulator layers. In this structure, when an in-plane (IP) current flows in the HM layer, a pure spin current can be generated and, therefore, exert torques on the FM layer. The current-induced SOTs are believed to originate from the spin Hall effect (SHE)[5,6] of the HMs or/and the Rashba effect.[7] The SOT can be divided into two mutually orthogonal components, the damping- and field-like torques. Importantly, the magnetization can be switched by the damping-like torque with the assistance of an external magnetic field for the perpendicularly magnetized structures based on the heavy metals with large spin Hall angles (θ_{SHE}), such as Ta,[4,8–14] Pt,[15–23] and W.[24]

More recently, studying the SOTs in the antiferromagnet (AFM)-based structures has become a promising direction, due to the exotic properties of the AFMs, e.g., the insensitivity to magnetic field, the lack of stray field[25] and excellent high-frequency properties.[26] The spin Hall angles in different AFMs of FeMn,[27,28] PdMn,[28,29] IrMn,[28,30–33] and PtMn[28,34] have been studied in the previous experiments. A few experiments have further demonstrated the SOT-driven perpendicular magnetization switching in the AFM-based structures.[34–36] The development of utilizing the SOTs for magnetization switching is thus particularly interesting for applications.

In this work, the current-induced SOTs in a perpendicularly magnetized $Ir_{22}Mn_{78}$(IrMn)/$Co_{20}Fe_{60}B_{20}$(CoFeB)/MgO structure are investigated. The damping- and field-like torques are measured using the harmonic technique, and the spin Hall angle of IrMn is obtained. Subsequently, the SOT-driven magnetization switching is demonstrated with the assistance of an external in-plane field. The polar magneto-optical Kerr effect (MOKE) imaging experiments reveal that the switching is achieved via current-driven domain nucleation and domain wall (DW) motion processes.

The films consisting of IrMn(5)/CoFeB(1)/MgO/Ta(1) (thicknesses in nm) were grown by magnetron sputtering at room temperature on Si substrates capped with 100 nm thermal oxide. The base pressure of the sputtering chamber is lower than 2×10^{-8} Torr. The films were annealed at 250 °C in vacuum under an out-of-plane (OOP) field. In order to investigate the current-induced SOTs, the films were patterned into Hall bar devices using a standard photolithography and dry etching technique. All the measurements were carried out at room temperature.

The micrograph of the device and the measurement set-up are shown in the lower inset of Fig. 1(a). The dimensions of the current channel (in x-axis direction) are 11 μm × 38 μm. The in-plane (IP) and out-of-plane (OOP) hysteresis loops were measured by anomalous Hall effect (AHE), as shown in Fig. 1. As we know, the AHE resistance is proportional to the perpendicular magnetization component (in our case, the anomalous Hall coefficient is negative, i.e., $R_{AHE} \propto -M_z$). The abrupt switching in the OOP direction verifies that the easy axis is in the OOP direction. The OOP hysteresis loop in low field region is shown in the upper inset. A large exchange bias field, H_{EB}, of -290 Oe is obtained, which favors $M_z > 0$ (i.e., $R_{AHE} < 0$) direction. The out-of-plane exchange bias also has an influence on the IP loop. When sweeping an IP magnetic field, the anomalous resistance is always negative, indicating $M_z > 0$, which is favored by the out-of-plane exchange bias.

Next, we investigate the current-induced SOTs using the well-established harmonic technique.[8,9,17,37] The measurement details are presented as following: A small sinusoidal current ($I = I_{ac} \sin(2\pi ft)$, which has peak value of I_{ac} and

a)Email: guoqiangyu@ucla.edu

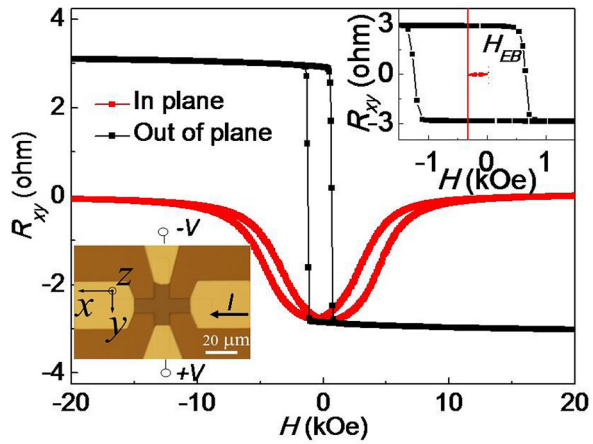

FIG. 1. The anomalous Hall resistance (R_{xy}) was measured with the in-plane (red) and out-of-plane field (black). The upper inset shows the exchange bias field, H_{EB}, for the out-of-plane loop. The lower inset shows the micrograph of the Hall bar device with schematic illustrations of the Hall measurement set-up.

frequency of $f = 133.33$ Hz), is applied along the current channel, as shown in the inset of Fig. 1. For the longitudinal (transverse) measurement, we sweep the IP magnetic field, $H_{x(y)}$, along the current (voltage) channel. The first and second harmonic signals are detected by a lock-in technique. The first harmonic V_ω and the second harmonic voltage $V_{2\omega}$ are expressed as[8]

$$V_\omega = \frac{R_{xy}}{2}\left(1 - \frac{A}{2D^2}\right)\Delta I, \quad V_{2\omega} = \frac{1}{2}\frac{R_{xy}}{2}\frac{B}{2D^2}\Delta I, \qquad (1)$$

$A = H_x^2 \sin^2\varphi + H_y^2 \cos^2\varphi + 2H_xH_y \cos\varphi \sin\varphi$, $B = 2H_x\Delta H_x \sin^2\varphi + 2H_y\Delta H_y \cos^2\varphi + 2(H_x\Delta H_x + H_y\Delta H_y)\cos\varphi \sin\varphi$, $D = (2K_u/M_s) - 4\pi M_s + H_{EB}$, where K_u denotes the perpendicular magnetic anisotropy constant, ΔI is the magnitude of sinusoidal current, φ is the azimuthal angle (with respect to y axis) of magnetization, and M_S denotes the saturation magnetization of the ferromagnetic layer. When the in-plane external field is applied along the transverse (longitudinal) direction, the angle value is $\varphi = 0$ ($\pi/2$). The damping-like (ΔH_x) and field-like (ΔH_y) effective fields can be obtained by the following equations:[8]

$$\Delta H_{x(y)} = -2\frac{\partial V_{2\omega}}{\partial H_{x(y)}} \Big/ \frac{\partial^2 V_\omega}{\partial H_{x(y)}{}^2}. \qquad (2)$$

We point out that Eq. (2) is obtained when the perpendicular exchange bias field is considered. The planar Hall resistance in this structure is ~0.09 Ω, which is negligible compared with the anomalous Hall resistance ~3.0 Ω (see Fig. 1). Therefore, we neglect the contribution of the planar Hall effect to the longitudinal and transverse effective fields.[38,39]

Figures 2(a)–2(d) show the first and second harmonic results for the external field along the current and voltage channels, respectively. $\partial V_{2\omega}/\partial H_{x(y)}$ is obtained by linearly fitting the second harmonic signal. $\partial^2 V_\omega/\partial H_{x(y)}^2$ is obtained by fitting the first harmonic signal using a parabolic function. The best fittings (red solid lines) are shown in Figs. 2(a)–2(d). The effective fields are obtained based on Eq. (2). Figure 2(e) shows the current density dependence of the damping- and field-like effective fields. Here, we calculate the current density based on the measured resistivity of CoFeB and IrMn, which are 160 and 278 $\mu\Omega$ cm, respectively. The corresponding current density in IrMn for $I_{ac} = 1$ mA is $J_{ac} = 0.14 \times 10^7$ A/cm^2. The linear dependence of the effective fields on different current densities (except for the $J_{ac} = 0.95 \times 10^7$ A/cm^2) indicates that the nonlinear effects are negligible in lower currents. When the current density is 0.95×10^7 A/cm^2, nonlinear effects, such as current-induced Joule heating,[8] may have a contribution to the effective fields. From the linear relationship, the effective damping- and field-like torque efficiency, defined by $\Delta H/J_{ac}$, are 1.84 and 0.71 mT per 10^7 A/cm^2, respectively.

Assuming the damping-like torque is solely originated from the spin Hall effect, the spin Hall angle can be obtained from the damping-like field using[40] $\theta_{SHE} = -\frac{2|e|M_S t_F}{\hbar} \times \frac{\Delta H_x}{J_{ac}}$, where $|e|$ and t_F represent the absolute value of electron charge and ferromagnetic layer thickness, respectively, and M_S is determined to be ~1022 emu/cc measured by SQUID at room temperature. The obtained spin Hall angle of $Ir_{22}Mn_{78}$ is 0.057 ± 0.002, which is consistent with the previous reports.[30,33] The sign of the spin Hall angle of IrMn is the same as that of Pt,[14,23] but opposite to that of Ta.[4] The spin Hall angle of $Ir_{22}Mn_{78}$ is larger than the reported value of $Ir_{50}Mn_{50}$,[31] although the former has less heavy metal element Ir. This may suggest that the spin Hall effect in this material is not solely determined by the quantity of the heavy metal Ir.[41]

We next prove that current-induced Oersted field cannot account for the observed field-like effective field. The current-induced Oersted field can be expressed as[33] $H_{Oe} \approx I_{Oe}/2w$,

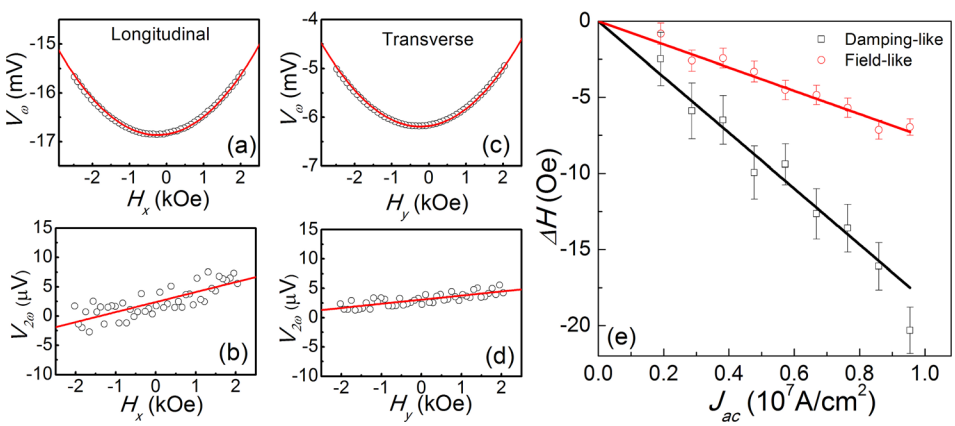

FIG. 2. The first and second harmonic anomalous signals for (a) and (b) longitudinal and (c) and (d) transverse measurement with $J_{ac} = 0.75 \times 10^7$ A/cm^2. H_x and H_y represent the external field along the current (x axis) and voltage (y axis) channel, respectively. (e) The current (peak value) dependence of field-like (red) and damping-like (black) effective field extracted by fitting the first and second harmonic signals, respectively. The solid lines in all figures show the best fitting results.

where I_{Oe} is the current in the IrMn layer and w is the width of the Hall bar ($w = 11\ \mu$m). The obtained field-like effective field is 2.4 times larger than the Oersted field (0.30 mT per 10^7 A/cm^2) induced by the current in IrMn layer. In addition, the former is in the opposite direction to the latter. Therefore, the observed field-like effective field cannot be attributed to the current-induced Oersted field. The field-like effective field may originate from the spin Hall effect[42] or/and the Rashba effect.[43] The observed field-like torque is smaller than those in Ta- (~2.5 mT per 10^7 A/cm^2)[13] and Pt- (~3.2 mT per 10^7 A/cm^2)[17] based structures.

In the following, we demonstrate that the SOT enables current-driven perpendicular magnetization switching. During the current sweeping, a constant in-plane field collinear with the current is applied, which is required for breaking the symmetry to realize deterministic switching.[19,44,45] Figures 3(a) and 3(b) show the current-driven magnetization switching with magnetic fields along positive and negative x directions. When a positive in-plane field is applied, a positive current switches the magnetization from $M_z > 0$ to $M_z < 0$. The favored magnetization direction is reversed when the in-plane field is reversed, which is a typical signature of SOT switching.[4,23] It should be noted that, for the switching from $M_z > 0$ to $M_z < 0$, the anomalous Hall resistance does not reach the maximum value, as obtained in the OOP hysteresis loop (see Fig. 1). This is mainly because of the incomplete switching at the cross section, due to the joint effect of the reduced current density and additional pinning effect at the cross section of the Hall bar, which will be discussed later based on the MOKE imaging experiments. The thermal effect may also reduce anomalous Hall resistance and/or generate a very small vertical offset in hysteresis loop, which however is believed to be non-significant. In principle, a larger current density should be able to realize complete switching. However, the device is burned when the applied current is larger than the maximum current shown in Fig. 3(a).

As illustrated in the switching phase diagram (SPD) in Fig. 3(c), the polarity of the switching indicates a positive spin Hall angle, which is consistent with the results of the harmonic measurements. In addition, we calculate the switching efficiency, $\eta = (H_k - H_x)/J_c$, where H_k and J_c are the anisotropy field (~10 kOe from IP loop, as shown in Fig. 1) and critical switching current density, respectively. The switching efficiency is determined to be ~4.2 kOe per 10^7 A/cm^2, which is comparable to those in Ta- (~4.3–5.5 kOe per 10^7 A/cm^2) and Pt- (~1.0–4.7 kOe per 10^7 A/cm^2) based systems.[20,46] The inset indicates the region (gray color) where the magnetization cannot be switched by the given currents. The narrow region, ~20 Oe, reveals that the switching can be realized with the assistance of a small external field. This feature may provide advantages when the external magnetic field is replaced by the in-plane exchange bias for the field-free SOT-driven switching,[35,47] since only a small external field is required to enable the switching. The narrow non-reversal region may be due to the weak Dzyaloshinskii-Moriya interaction (DMI), since the required minimum in-plane field for switching is correlated with the DMI strength.[11,45,48]

In order to investigate the process of SOT-driven magnetization switching, we performed polar MOKE imaging experiments. Figure 4 shows the observed magnetization configurations when different external magnetic fields and currents are applied. Here, the dark (light) area represents $M_z < 0$ ($M_z > 0$), respectively. First, we apply an out-of-plane magnetic field to align the magnetization to the $M_z < 0$ direction (see Fig. 4(a)). Then, an in-plane field, $H_x = 303$ Oe, and a negative pulse current density, $J = -1.76 \times 10^7$ A/cm^2, are

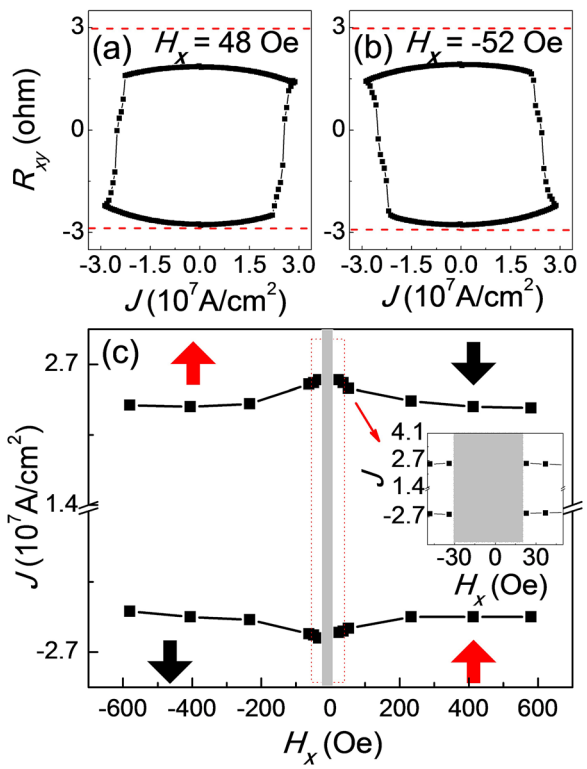

FIG. 3. The current-driven magnetization switching in the constant (a) negative and (b) positive fields. The red dash lines denote the anomalous Hall resistance when the magnetization is completely switched. (c) The switching phase diagram (SPD) for different in-plane fields. The inset shows the magnified SPD for low fields. The red and dark arrows in switching phase diagram represent the upward and downward magnetizations, respectively.

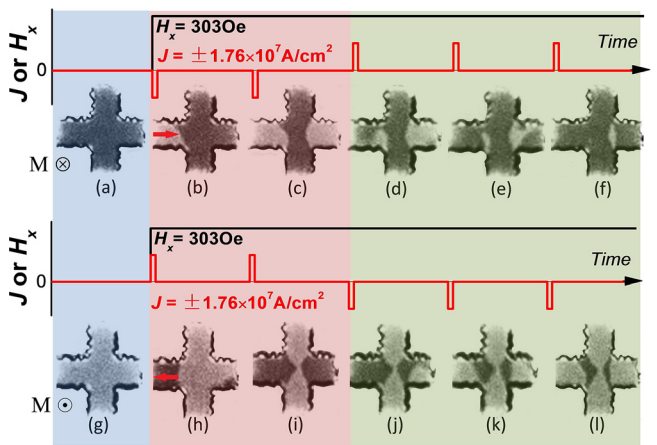

FIG. 4. The polar magneto-optical Kerr effect (MOKE) imaging experiments of current driven magnetization switching with the initial state of (a)–(f) $M_z < 0$ and (g)–(l) $M_z > 0$ when the positive in-plane field, $H_x = 303$ Oe, and the DC current density, $\pm 1.76 \times 10^7$ A/cm^2, were applied. The duration of the pulses is 1 s. The red arrows indicate the direction of first applied current pulse.

applied (negative sign denotes that the current flows to right). The MOKE images are captured after applying the current pulses with 1 s duration. The results indicate that the domain nucleation starts from the edges of the Hall bar, and the generated domain walls (DWs) propagate from the edges to the center of the device (see Figs. 4(b) and 4(c)). This observation shows that the applied in-plane magnetic field is large enough to overcome the chirality of domain wall, resulting in the deterministic reversal. We point out that, in the current channel, the switching is not completely achieved in the cross section of the Hall bar, even for a larger current. This is actually consistent with the results of the transport measurement. This may be due to either the lower current density (since the current path becomes wider at the cross section) or additional pinning effect from the cross section.[49] However, the complete switching is realized in the other regions of the current channel. Next, when we start to apply a positive current, the magnetization is switched back. Again, the switching is achieved through magnetization nucleation at the left and right edges and subsequent domain wall motion from edges to the center. As shown in Figs. 4(d)–4(f), the magnetization almost returns to the initial state, $M_z < 0$. Figures 4(g)–4(i) show the similar phenomenon with the $M_z > 0$ initial state. The polar MOKE images shown in Fig. 4 indicate that the switching takes place through domain nucleation and DW propagation.[11,50,51]

In summary, the SOTs are investigated in a perpendicularly magnetized IrMn/CoFeB/MgO structure. The damping- and field-like torques are measured by the harmonic technique, and the large spin Hall angle of IrMn is obtained to be around 0.057. The SOT-driven magnetization switching is realized with the assistance of an in-plane external magnetic field. The narrow non-reversal region will facilitate the switching because the switching can be realized with a small symmetry-breaking field. The polar Kerr imaging experiments show the magnetization switching process in details, which clearly demonstrates that the switching takes place through domain nucleation and domain wall motion. Hopefully, these experimental results can encourage more detailed researches and facilitate the design of SOT devices based on the AFM materials.

Note added in proof: We would like to state that we realized a similar work was done by another group when we were preparing the revised manuscript.[36] We pointed out that the exchange bias is out-of-plane in the studied materials, which is different from the previous studies, where the exchange bias is in-plane.[36]

This work was supported in part by C-SPIN and FAME, two of six centers of STARnet, a Semiconductor Research Corporation Program, sponsored by MARCO and DARPA. This work was also supported by the National Science Foundation (ECCS 1611570) and the Nanosystems Engineering Research Center for Translational Applications of Nanoscale Multiferroic Systems (TANMS) Cooperative Agreement Award No. EEC-1160504. We would like to acknowledge the collaboration of this research with the King Abdul-Aziz City for Science and Technology (KACST) via the Center of Excellence for Green Nanotechnologies (CEGN). This work was supported as part of the SHINES Center, an Energy Frontier Research Center funded by the U.S. Department of Energy, Office of Science, Basic Energy Sciences under Award No. S000686. D. Wu and Z. Z. Zhang would like to thank the support of China Scholarship Council (CSC), the 973 Program (2014CB921104) and the National Natural Science Foundation of China (NSFC) Grant (No. 11474067). In addition, G.Q.Y. acknowledges Junyang Chen for fruitful discussions.

[1]I. M. Miron, K. Garello, G. Gaudin, P. J. Zermatten, M. V. Costache, S. Auffret, S. Bandiera, B. Rodmacq, A. Schuhl, and P. Gambardella, Nature **476**, 189 (2011).
[2]K. L. Wang, J. G. Alzate, and P. Khalili Amiri, J. Phys. D: Appl. Phys. **46**, 074003 (2013).
[3]T. Jungwirth, J. Wunderlich, and K. Olejnik, Nat. Mater. **11**, 382 (2012).
[4]L. Q. Liu, C. F. Pai, Y. Li, H. W. Tseng, D. C. Ralph, and R. A. Buhrman, Science **336**, 555 (2012).
[5]J. E. Hirsch, Phys. Rev. Lett. **83**, 1834 (1999).
[6]S. F. Zhang, Phys. Rev. Lett. **85**, 393 (2000).
[7]Y. A. Bychkov and E. I. Rashba, JETP Lett. **39**, 78 (1984).
[8]J. Kim, J. Sinha, M. Hayashi, M. Yamanouchi, S. Fukami, T. Suzuki, S. Mitani, and H. Ohno, Nat. Mater. **12**, 240 (2013).
[9]C. O. Avci, K. Garello, C. Nistor, S. Godey, B. Ballesteros, A. Mugarza, A. Barla, M. Valvidares, E. Pellegrin, A. Ghosh, I. M. Miron, O. Boulle, S. Auffret, G. Gaudin, and P. Gambardella, Phys. Rev. B **89**, 214419 (2014).
[10]X. Qiu, P. Deorani, K. Narayanapillai, K. S. Lee, K. J. Lee, H. W. Lee, and H. Yang, Sci. Rep. **4**, 4491 (2014).
[11]G. Q. Yu, P. Upadhyaya, K. L. Wong, W. J. Jiang, J. G. Alzate, J. S. Tang, P. K. Amiri, and K. L. Wang, Phys. Rev. B **89**, 104421 (2014).
[12]D. Bhowmik, M. E. Nowakowski, L. You, O. Lee, D. Keating, M. Wong, J. Bokor, and S. Salahuddin, Sci. Rep. **5**, 11823 (2015).
[13]C. Zhang, S. Fukami, H. Sato, F. Matsukura, and H. Ohno, Appl. Phys. Lett. **107**, 012401 (2015).
[14]D. Wu, G. Q. Yu, Q. M. Shao, X. Li, H. Wu, K. L. Wong, Z. Z. Zhang, X. F. Han, P. K. Amiri, and K. L. Wang, Appl. Phys. Lett. **108**, 212406 (2016).
[15]W. F. Zhang, W. Han, X. Jiang, S. H. Yang, and S. S. P. Parkin, Nat. Phys. **11**, 496 (2015).
[16]M. H. Nguyen, D. C. Ralph, and R. A. Buhrman, Phys. Rev. Lett. **116**, 126601 (2016).
[17]K. Garello, I. M. Miron, C. O. Avci, F. Freimuth, Y. Mokrousov, S. Blugel, S. Auffret, O. Boulle, G. Gaudin, and P. Gambardella, Nat. Nanotechnol. **8**, 587 (2013).
[18]C. Bi, L. Huang, S. B. Long, Q. Liu, Z. H. Yao, L. Li, Z. L. Huo, L. Q. Pan, and M. Liu, Appl. Phys. Lett. **105**, 022407 (2014).
[19]J. C. Rojas-Sánchez, P. Laczkowski, J. Sampaio, S. Collin, K. Bouzehouane, N. Reyren, H. Jaffrès, A. Mougin, and J. M. George, Appl. Phys. Lett. **108**, 082406 (2016).
[20]J. W. Yu, X. P. Qiu, W. Legrand, and H. Yang, Appl. Phys. Lett. **109**, 042403 (2016).
[21]C. Bi and M. Liu, J. Magn. Magn. Mater. **381**, 258 (2015).
[22]M. Yang, K. Cai, H. Ju, K. W. Edmonds, G. Yang, S. Liu, B. Li, B. Zhang, Y. Sheng, S. Wang, Y. Ji, and K. Wang, Sci. Rep. **6**, 20778 (2016).
[23]L. Liu, O. J. Lee, T. J. Gudmundsen, D. C. Ralph, and R. A. Buhrman, Phys. Rev. Lett. **109**, 096602 (2012).
[24]Q. Hao and G. Xiao, Phys. Rev. Appl. **3**, 034009 (2015).
[25]B. Howells, P. Wadley, J. Železný, C. Andrews, V. Hills, R. P. Campion, K. Olejník, V. Novák, F. Maccherozzi, S. S. Dhesi, S. Y. Martin, T. Wagner, F. Freimuth, J. Wunderlich, Y. Mokrousov, J. Kuneš, J. S. Chauhan, A. W. Rushforth, M. J. Grzybowski, K. W. Edmonds, B. L. Gallagher, and T. Jungwirth, Science **351**, 587 (2016).
[26]T. Kampfrath, A. Sell, G. Klatt, A. Pashkin, S. Mahrlein, T. Dekorsy, M. Wolf, M. Fiebig, A. Leitenstorfer, and R. Huber, Nat. Photonics **5**, 31 (2011).
[27]Y. M. Yang, Y. J. Xu, X. S. Zhang, Y. Wang, S. F. Zhang, R. W. Li, M. S. Mirshekarloo, K. Yao, and Y. H. Wu, Phys. Rev. B **93**, 094402 (2016).
[28]W. Zhang, M. B. Jungfleisch, W. Jiang, J. E. Pearson, A. Hoffmann, F. Freimuth, and Y. Mokrousov, Phys. Rev. Lett. **113**, 196602 (2014).
[29]W. Zhang, M. B. Jungfleisch, F. Freimuth, W. J. Jiang, J. Sklenar, J. E. Pearson, J. B. Ketterson, Y. Mokrousov, and A. Hoffmann, Phys. Rev. B **92**, 144405 (2015).

[30]J. B. S. Mendes, R. O. Cunha, O. Alves Santos, P. R. T. Ribeiro, F. L. A. Machado, R. L. Rodríguez-Suárez, A. Azevedo, and S. M. Rezende, Phys. Rev. B **89**, 140406 (2014).
[31]W. Han, W. F. Zhang, S. H. Yang, Y. Sun, Y. Zhang, B. H. Yan, and S. S. P. Parkin, Sci. Adv, **2**, e1600759 (2016).
[32]H. Reichlová, D. Kriegner, V. Holý, K. Olejník, V. Novák, M. Yamada, K. Miura, S. Ogawa, H. Takahashi, T. Jungwirth, and J. Wunderlich, Phys. Rev. B **92**, 165424 (2015).
[33]V. Tshitoyan, C. Ciccarelli, A. P. Mihai, M. Ali, A. C. Irvine, T. A. Moore, T. Jungwirth, and A. J. Ferguson, Phys. Rev. B **92**, 214406 (2015).
[34]Y. X. Ou, S. J. Shi, D. C. Ralph, and R. A. Buhrman, Phys. Rev. B **93**, 220405 (2016).
[35]S. Fukami, C. Zhang, S. DuttaGupta, A. Kurenkov, and H. Ohno, Nat. Mater. **15**, 535 (2016).
[36]Y. W. Oh, S. H. Chris Baek, Y. M. Kim, H. Y. Lee, K. D. Lee, C. G. Yang, E. S. Park, K. S. Lee, K. W. Kim, G. Go, J. R. Jeong, B. C. Min, H. W. Lee, K. J. Lee, and B. G. Park, Nat. Nanotechnol. **11**, 878 (2016).
[37]C. O. Avci, K. Garello, M. Gabureac, A. Ghosh, A. Fuhrer, S. F. Alvarado, and P. Gambardella, Phys. Rev. B **90**, 224427 (2014).
[38]M. Hayashi, J. Kim, M. Yamanouchi, and H. Ohno, Phys. Rev. B **89**, 144425 (2014).
[39]H. R. Lee, K. Lee, J. Cho, Y. H. Choi, C. Y. You, M. H. Jung, F. Bonell, Y. Shiota, S. Miwa, and Y. Suzuki, Sci. Rep. **4**, 6548 (2014).
[40]A. V. Khvalkovskiy, V. Cros, D. Apalkov, V. Nikitin, M. Krounbi, K. A. Zvezdin, A. Anane, J. Grollier, and A. Fert, Phys. Rev. B **87**, 020402 (2013).
[41]H. Chen, Q. Niu, and A. H. MacDonald, Phys. Rev. Lett. **112**, 017205 (2014).
[42]X. Fan, J. Wu, Y. Chen, M. J. Jerry, H. Zhang, and J. Q. Xiao, Nat. Commun. **4**, 1799 (2013).
[43]I. M. Miron, G. Gaudin, S. Auffret, B. Rodmacq, A. Schuhl, S. Pizzini, J. Vogel, and P. Gambardella, Nat. Mater. **9**, 230 (2010).
[44]G. Q. Yu, P. Upadhyaya, Y. Fan, J. G. Alzate, W. Jiang, K. L. Wong, S. Takei, S. A. Bender, L. T. Chang, Y. Jiang, M. Lang, J. Tang, Y. Wang, Y. Tserkovnyak, P. K. Amiri, and K. L. Wang, Nat. Nanotechnol. **9**, 548 (2014).
[45]O. J. Lee, L. Q. Liu, C. F. Pai, Y. Li, H. W. Tseng, P. G. Gowtham, J. P. Park, D. C. Ralph, and R. A. Buhrman, Phys. Rev. B **89**, 024418 (2014).
[46]L. M. Loong, P. Deorani, X. P. Qiu, and H. Yang, Appl. Phys. Lett. **107**, 022405 (2015).
[47]A. van den Brink, G. Vermijs, A. Solignac, J. Koo, J. T. Kohlhepp, H. J. Swagten, and B. Koopmans, Nat. Commun. **7**, 10854 (2016).
[48]C. F. Pai, M. H. Nguyen, C. Belvin, L. H. Vilela-Leão, D. C. Ralph, and R. A. Buhrman, Appl. Phys. Lett. **104**, 082407 (2014).
[49]E. Martinez, L. Torres, and L. Lopez-Diaz, Phys. Rev. B **83**, 174444 (2011).
[50]S. Pizzini, J. Vogel, S. Rohart, L. D. Buda-Prejbeanu, E. Jue, O. Boulle, I. M. Miron, C. K. Safeer, S. Auffret, G. Gaudin, and A. Thiaville, Phys. Rev. Lett. **113**, 047203 (2014).
[51]E. Martinez, L. Torres, N. Perez, M. A. Hernandez, V. Raposo, and S. Moretti, Sci. Rep. **5**, 10156 (2015).